Inorganic Chemistry

Article

pubs.acs.org/IC

Low-Temperature Nitridation of Manganese and Iron Oxides Using $NaNH_2$ Molten Salt

Akira Miura,* Takahiro Takei, and Nobuhiro Kumada

Center for Crystal Science and Technology, University of Yamanashi, 7-32 Miyamae, Kofu, Yamanashi 400-8511, Japan

ABSTRACT: Manganese and iron nitrides are important functional materials, but their synthesis processes from oxides often require high temperatures. Herein, we show a novel meta-synthesis method for manganese and iron nitrides by low-temperature nitridation of their oxides using $NaNH_2$ molten salt as the nitrogen source in an autoclave at 240 °C. With this method, nitridation of micrometer-sized oxide particles kept their initial morphologies, but the size of the primary particles decreased. The thermodynamic driving force is considered to be the conversion of oxides to sodium hydroxide, and the kinetic of nitridation is improved by the decrease of particle size and the low melting point of $NaNH_2$. This technique as developed here has the advantages of low reaction temperature, reduced consumption of ammonia, employing nonspecialized equipment, and providing facile control of the reactions for producing nitrides from oxides.

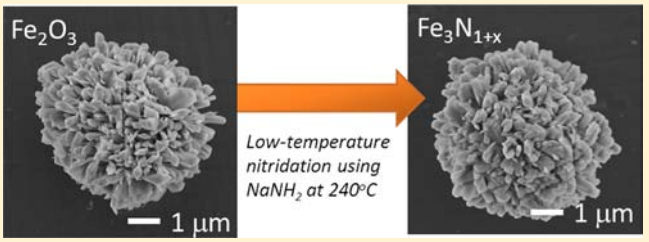

INTRODUCTION

Transition-metal nitrides have enormous potential because of their unique physical and chemical properties.[1] Among them, manganese and iron nitrides are important functional materials as catalysts,[2] photocatalysts,[3] magnetic materials,[4,5] and negative thermal expansion materials.[6] However, the synthesis procedures for nitrides mostly require high-temperature treatment above 300 °C, and the use of a large amount of nitrogen sources, such as toxic ammonia.[2−7] Metasynthesis routes are strong candidates to reduce synthesis temperature and consumption of nitrogen sources. Typically, meta-synthesis involves reactions between metal halides and nitrogen sources such as Li_3N, NaN_3, or $NaNH_2$ in an inert atmosphere or dry organic solvents.[8] The driving forces of metasynthesis are the formation of byproducts, like LiCl or NaI. Nonetheless, low-temperature metasynthesis of nitrides from oxides has rarely been reported, even though oxides are important precursors with less toxicity, show good cost performance, and are available in a variety of compositions, structures, and morphologies. This could be because low-temperature nitridation of oxides faces both thermodynamic and kinetic challenges. The much higher formation energies of oxides compared to those of nitrides make nitridation difficult, and low temperatures cannot always provide a moderate reaction rate to complete nitridation in a reasonable time. Sodium amide, $NaNH_2$, is an attractive nitrogen source for the synthesis of nitrides[9] because of its low melting point of about 210 °C. Titanium nitride, TiN, can be obtained by the reaction of TiO_2 with $NaNH_2$, but its nitridation temperature is 500−600 °C.[10] Recently, $NaNH_2$ flux was found to convert $LiInO_2$ particles into InN nanocrystals in an autoclave as low as 240 °C.[11] This finding motivates us to explore the synthesis of other functional nitrides by low-temperature nitridation of other oxides, using $NaNH_2$ as the nitrogen source.

Herein, we report the low-temperature nitridation of Mn_2O_3 and Fe_2O_3 using $NaNH_2$ molten salt at 240 °C. Manganese and iron nitrides were synthesized from micrometer-sized oxide particles. We propose a pseudomorphous nitridation mechanism, which differs from that stated in a previous report regarding the low-temperature nitridation of $LiInO_2$ using $NaNH_2$ flux.[11] We discuss the low-temperature nitridation in terms of kinetics and thermodynamics, and clarify the advantages of our approach over high-temperature nitridation between oxides under a continuous ammonia flow.

EXPERIMENTAL DETAILS

The following chemicals were used without further treatment; Mn_2O_3 (Aldrich >99%), Fe_2O_3 powder (Kojyundo Kagaku >99.9%), $NaNH_2$ powder (Aldrich >95%). ***Caution!*** *Sodium amide powder ($NaNH_2$) is highly sensitive to air and moisture, flammable, and can cause burns. It should be handled in a glovebox.*

Oxide powder (0.20 g) and $NaNH_2$ (1.0 g) were put in a steel crucible, which was then placed in a Teflon-lined steel autoclave inside a nitrogen-filled glovebox. The autoclave was tightly closed and kept in an oven at 240 °C for 36 h. After the autoclave was cooled down, it was opened and exposed to a normal atmosphere. Ethanol was added into the crucible, and the solution was stirred by a magnetic stirrer until excess $NaNH_2$ and byproducts were dissolved. The manganese product was collected by filtration, and washed with water, and then dried overnight at room temperature. The iron products were collected by a permanent magnet and washed with ethanol.

Crystal structure analysis was performed by powder X-ray diffraction (XRD) patterns using an RINT-2000 (Rigaku; CuKα radiation) system. The scan was performed over the range of 20−70° or 20−80° with a step of 0.02°. The *d* values of the indexed peaks were obtained and used to calculate the lattice parameters via the method of least-squares. Morphologies were investigated by scanning electron

Received: April 30, 2013
Published: September 27, 2013

microscopy (FE-SEM; JEOL; JSM-6500) and transition electron microscopy (TEM; FEI; Tecnai Osiris). Elementary analysis was performed by inductively coupled plasma atomic emission spectrometry (ICP-AES; Seiko; SPS1700), atomic absorption spectroscopy (AAS; Shimazu; AA-6800), CHN analysis (Yanako; MT-6), and oxygen analysis (LECO; TC-600). Surface analysis was performed by X-ray photoelectron spectroscopy (XPS: JEOL; JPS-9200). In situ etching was performed with an Ar ion supply operated at 3 keV. The bonding energies were corrected by reference to free carbon (284.6 eV). The magnetic susceptibilities at 300 K were measured using a superconductive quantum interference device (SQUID; Quantum Design; MPMS-5S). Crystal structures were drawn using VESTA.[12]

RESULTS AND DISCUSSION

The XRD pattern of Mn_2O_3 powder after the nitridation using $NaNH_2$ at 240 °C is shown in Figure 1. The powder after the

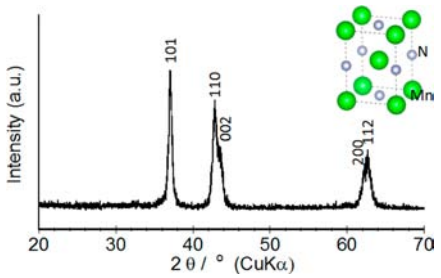

Figure 1. XRD pattern of Mn_6N_{5+x} synthesized from Mn_2O_3 particles. ICSD pattern of tetragonal rock-salt type of MnN (#106932) was used for the assignment.

nitridation can be assigned the tetragonal rock-salt structure of θ-Mn_6N_{5+x} with lattice parameters of a = 2.985(3) Å and c = 4.156(4) Å. These lattice parameters closely resemble previous values for MnN (a = 3.009 Å, c = 4.189 Å).[13] The slight difference may be attributed to the nonstoichiometry or oxygen incorporation. The crystalline size was determined to be about 20 nm from the 101 diffraction peak using the Scherrer equation.

SEM images before and after the nitridation are shown in Figure 2. The Mn_2O_3 powders comprised irregular particles of

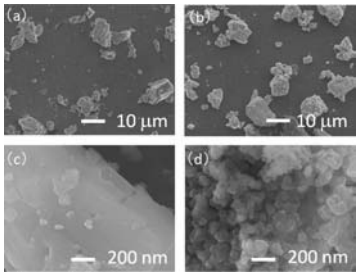

Figure 2. Low-magnification SEM images of Mn_2O_3 powder (a) before and (b) after nitridation. High-magnification images of Mn_2O_3 powder (c) before and (d) after nitridation.

up to 20 μm in size with similar morphologies, both before and after nitridation (Figure 2(a, b)). However, upon nitridation, the smooth surface became rough, with small particles of less than 200 nm (Figure 2(c, d)). Thus, this low-temperature nitridation is considered a pseudomorphous reaction, which retains the initial morphologies by aggregation of smaller particles. TEM images are not shown because electron beam irradiation during the observations likely caused decomposition of the synthesized nitrides.

To examine the surface and inner nitride particles, elemental and surface analyses were performed. Manganese, nitrogen, and oxygen contents of the synthesized nitride after the washing were 83(7) wt %, 18(1) wt %, 2.8(3) wt %, respectively. The molar ratio of Mn:N:O was approximately 1.00:0.86:0.12, suggesting the formation of Mn_6N_{5+x} with an oxide surface and/or incorporation of oxygen. Either no or only small amounts of carbon, hydrogen, and sodium were detected (<0.2 wt %). XPS results of the nitride powder before and after Ar etching showed a doublet for Mn2p and singlets for N1s and O1s (Figure 3). The energies of Mn2p doublet peaks were

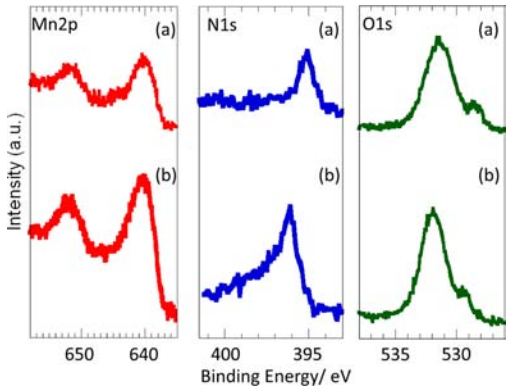

Figure 3. Mn2p, N1s, and O1s XPS spectra of manganese nitride powder (a) before and (b) after three-minute Ar etching.

almost the same energies before (640.4 and 652.0 eV) and after Ar etching (640.3 and 652.1 eV), which were close to the reported values of Mn−N in Mn-doped GaN.[14] The peak positions of N1s before and after etching were 395.1 eV and 396.2 eV, respectively, which could be explained by N−N bonding on the surface[15] and metal−N bonding,[16] respectively. The O1s peak changed from a broad peak at 531.5 eV with a shoulder at 528.6 eV before etching into a sharp peak at 531.9 eV with a shoulder at 529.5 eV. Literature values for O^{2-}, Mn−O, and O−H bonding energies are 528,[17] 529−530,[18] and 532 eV,[19,20] respectively, indicating Ar etching removed the adsorbed oxygen on the surface of the nitrides. Consequently, the surface of the nitride after washing with water was most probably covered with adsorbed N/O, oxides, and hydroxides. However, the possibility that oxygen is incorporated in the nitride phase cannot be denied when considering that oxynitrides with rock-salt structures have been reported.[21]

The magnetization of manganese nitride almost linearly increased with increasing magnetic field (Figure 4). This linear relationship and the order of susceptibility agree with previous reports about θ-Mn_6N_{5+x}, and suggest the possibility of antiferromagnetic behavior.[13,22]

The XRD pattern of Fe_2O_3 powders after the nitridation is shown in Figure 5. The product can be indexed as hexagonal ε-Fe_3N_{1+x} with lattice parameters of a = 4.706(9) Å and c = 4.370(6) Å. These lattice parameters are consistent with the reported values of ε-Fe_3N_{1+x}, with the nitrogen excess, x, estimated to be 0.0−0.1.[23] The crystalline size calculated by the Scherrer equation is approximately 15 nm. There is a broad peak around 35°, indicating the presence of low-crystalline or amorphous phases.

dx.doi.org/10.1021/ic401951u | Inorg. Chem. 2013, 52, 11787−11791

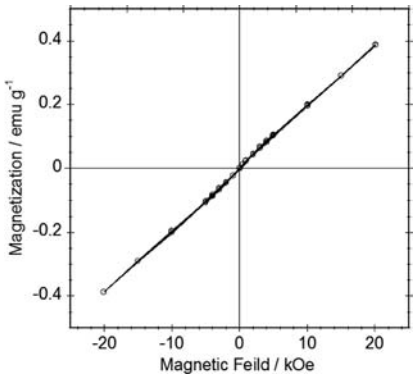

Figure 4. Magnetic property of manganese nitride powder at 300 K.

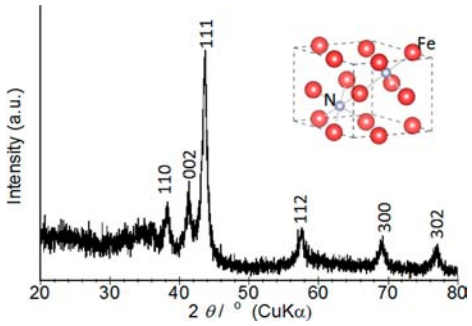

Figure 5. XRD pattern of Fe_3N_{1+x} synthesized from Fe_2O_3. ICSD pattern of ε-Fe_3N_{1+x} (#79983) was used for the assignments.

The SEM images before and after the nitridation are shown in Figure 6. The Fe_2O_3 powder after nitridation retains a

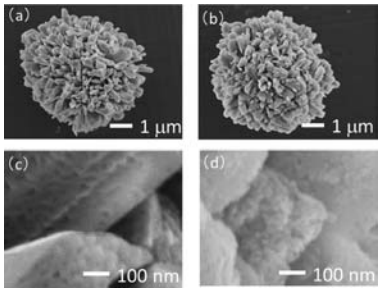

Figure 6. Low-magnification SEM images of Fe_2O_3 powder (a) before and (b) after nitridation. High-magnification images of Fe_2O_3 powder (c) before and (d) after nitridation.

flower-like morphology (Figure 6(a, b)). However, the nitridation decreases the size of primary particles from about 30 nm (Figure 6(c)) to about 20 nm (Figure 6(d)). Thus, this pseudomorphous feature is similar to the case of the nitridation of manganese oxide. Similar to manganese nitride, iron nitride, too, was not stable under TEM.

The iron and nitrogen contents were 66(6) and 7.0(1) wt %, respectively, with the molar ratio of Fe:N being approximately 1.00:0.42. Nonetheless, oxygen (24(2) wt %), carbon (~l wt %), hydrogen (~0.5 wt %), and sodium (~l wt %) were detected as impurities. Thus, we could not determine the component in the iron nitride phase and low-crystalline/amorphous impurities, such as oxides, oxynitrides, hydrocarbon, and hydroxides. The XPS results before and after 3 min of Ar-ion etching are shown in Figure 7. Two Fe 2p doublet peaks are observed at almost identical energies (708.8–709.0 and 722.0–

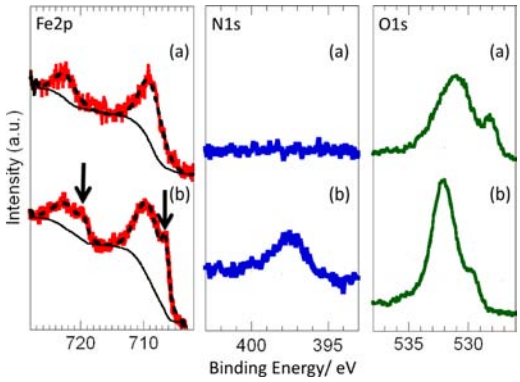

Figure 7. Fe 2p, N1s, and O1s XPS spectra of iron nitride powders synthesized from Fe_2O_3 particles (a) before and (b) after three-minute Ar etching with the reported binding energies of Fe_3N. Black lines are guides for the eye, and arrows indicate the shoulders agreeing with the reported values of Fe_3N.

722.3 eV) before and after Ar etching, which correspond to the energies of Fe_2O_3.[19,20] Nonetheless, only after etching are the shoulders at lower energies (706.5 and 719.5 eV) visible, which match the peak energies of Fe_3N.[19] Therefore, we consider that the iron nitride particles are covered with oxide and/or hydroxide layers. This is confirmed by the N1s peak at 397.5 eV after etching, which corresponds to that of iron nitride.[19] The O1s changed from a broad peak at 531.1 eV with a shoulder at 528.2 eV before etching into a sharp peak at 532.3 eV with a shoulder at 529.8 eV after etching. Literature values for adsorbed O^{2-}, Fe–O, O–H, and C–O bonding energies are 528,[17] 530,[19,20] 532,[19,20] and 533 eV, respectively, indicating that the etching removed the adsorbed oxygen on the surface of nitrides. These analyses suggest that Fe_3N_{1+x} nanocrystals are covered with adsorbed oxygen, low-crystalline oxides, oxynitrides, hydroxides, hydrocarbon, and/or sodium species, thus explaining the broad peak in the XRD pattern and the compositional deviation between chemical analysis and X-ray measurement. Even though the synthesized iron nitride was obtained after washing with ethanol, washing with water caused decomposition to iron oxide. Therefore, these impurities are probably formed by the reoxidation of the synthesized nitride considering its instability in water.

The magnetic hysteresis loop is shown in Figure 8. The magnetization at 50 kOe and magnetic coercivity of iron nitride powder were 29.2 emu/g and 70 Oe, respectively. These values are smaller than those of Fe_3N powder (135 emu/g at 10 kOe and 540 Oe).[24] When compared with Fe_3N nanoparticles, the

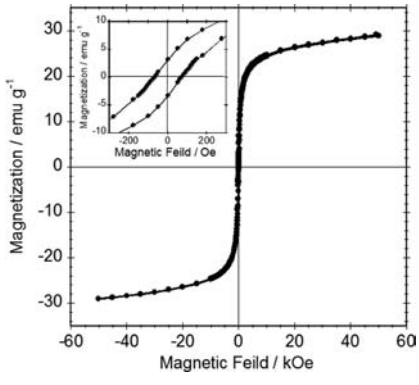

Figure 8. Magnetic property of iron nitride powder at 300 K.

dx.doi.org/10.1021/ic401951u | Inorg. Chem. 2013, 52, 11787–11791

magnetization is smaller than that reported in Fe_3N nanoparticles (51 emu/g),[25] but coercivity closely resembles the previous value (58 Oe).[25] Thus, obtained values of magnetization and coercivity could be attributed to nanosized crystalline feature of Fe_3N_{1+x} and the presence of impurity phases.

Here, we discuss how this low-temperature nitridation overcomes the kinetic barrier and satisfies thermodynamic requirements. Kinetics is a key factor, especially for low-temperature reactions, and it is known that reactions in the solution phase proceed at a higher reaction rate. Since $NaNH_2$ melts above 210 °C, it should increase the kinetics. In addition, this nitridation produces smaller particles, which can be explained by the replacement of oxygen atoms with less nitrogen atoms. Since nitridation involves diffusion of both nitrogen and oxygen, the large surface area of the smaller particles should enhance the low-temperature nitridation. Additionally, the low temperature can inhibit the growth of particles. The pseudomorphous reaction of micrometer-sized particles is an interesting feature. This is common in high-temperature ammonolysis of oxides under ammonia flow, as previously reported for Ta_3N_5[26] and MoN,[27] which differs from reported low-temperature nitridation of $LiInO_2$ using $NaNH_2$; that is, the reported nitridation results in hexagonal crystal morphologies from irregular-shaped oxides.[11] Evidence for a crystallographically topotactic reaction could not be obtained because of the instability feature during TEM observation.

These reactions probably involve the formation of hydroxides, such as NaOH.[10,11] Thus, the nitridation can be formulated as below:

$$1.5Mn_2O_3 + 4.5NaNH_2 \rightarrow Mn_3N_2 + 4.5NaOH + 0.5N_2 + 1.5NH_3 \quad (1)$$

$$1.5Fe_2O_3 + 4.5NaNH_2 \rightarrow Fe_3N + 4.5NaOH + N_2 + 1.5NH_3 \quad (2)$$

As described before, nitrides have relatively small formation energies when compared with oxides. The Gibbs free energy (ΔG_f) of manganese nitride, Mn_3N_2, at 298 K is −146.4 kJ/mol,[28] and those of $NaNH_2$ and NH_3 are −64.0 kJ/mol[29] and −16.4 kJ/mol,[29] respectively. The free energy of Fe_3N is estimated as −30 kJ/mol.[5,30] The nitrogen contents and crystal structures of these nitrides may be different from those of the products synthesized by this low-temperature method. However, we think that this deviation does not influence the thermodynamic estimation of these reactions because the ΔG_f values of oxides and hydroxides at 298 K are about one order magnitude higher: Fe_2O_3, −744.8 kJ/mol;[29] Mn_2O_3, −881.1 kJ/mol;[29] NaOH, −379.49 kJ/mol.[29] These energies indicate that the thermodynamic of the reactions should be governed by the formation of NaOH from transition-metal oxides. The free energies (ΔG_{rxn}) of the reactions 1 and 2 at 298 K are calculated to be −357 kJ and −269 kJ, respectively. It can be argued that a decrease in ΔG_{rxn} at 513 K will be found as these reactions produce gaseous products. Additionally, the Helmholtz free energy, ΔA_{rxn}, which is an important function of state under constant volume conditions, is more negative than ΔG_{rxn} since gaseous products cause an increase in pressure ($A = G - PV$). Accordingly, these low-temperature reactions 1 and 2 should be thermodynamically possible. Therefore, we believe that our method is a thermodynamically favorable meta-synthesis route, and its driving force is the formation of NaOH. This driving force creates the potentials to extend this low-temperature method to the synthesis of other transition-metal nitrides/oxynitrides and/or unreported nitrides/oxynitrides with relatively small formation energies.

In contrast to the reactions 1 and 2, the reaction with less $NaNH_2$ may prevent reactions:

$$1.5Mn_2O_3 + 2NaNH_2 \rightarrow Mn_3N_2 + 2NaOH + H_2O + 0.5O_2 \quad (3)$$

$$1.5Fe_2O_3 + NaNH_2 \rightarrow Fe_3N + NaOH + H_2O + 2.5O_2 \quad (4)$$

The ΔG_{rxn} values of the reactions 3 and 4 at 298 K are +307 and +162 kJ, respectively, which are more positive than those of reactions 1 and 2. Experimental results of the nitridation using a low ratio of $NaNH_2$ (0.05−0.1 g) to oxides (0.2 g) exhibited no or small diffraction peaks from nitrides. Thus, excess $NaNH_2$ is necessary to fulfill the thermodynamic requirement for this low-temperature nitridation.

The driving forces and kinetic control for the proposed method are different from those for the traditional high-temperature nitridation of oxides under continuous ammonia flow. One of the driving forces of the high-temperature conversion is the sweeping away of H_2O formed as the byproduct with flowing ammonia gas.[28] The rate of ammonia flow and heating time are often critical factors that control the nitridation.[31] Thus, high-temperature ammonolysis of oxides needs a considerably large amount of ammonia gas to purge the byproduct and control the nitridation. In contrast, our low-temperature nitridation uses H_2O to progress the nitridation by reaction with excess $NaNH_2$, and therefore, ammonia flow is not necessary. Although the reaction needs excess $NaNH_2$, the amount of ammonia consumed is one order smaller when 1.0 g of $NaNH_2$ is compared with the usage of an ammonia flow with a rate of 55 mL/min for 3 h[28] ($NaNH_2$:NH_3 = 1:17). Therefore, this low-temperature technique has the potential for reduced usage of ammonia combined with control of nitridation in a closed system without the need to tune the flow rate and time of ammonia gas.

CONCLUSIONS

The reactions of Mn_2O_3 and Fe_2O_3 with excess $NaNH_2$ gave access to their nitrides at 240 °C. The advantages of this route are facile control of the reactions by employing low reaction temperature, only the need for simple apparatuses, and the use of inexpensive and less toxic starting materials. Micrometer-sized oxide particles were pseudomorphously converted into nitride particles of θ-Mn_6N_{5+x} and ε-Fe_3N_{1+x} phases. The surface of the nitrides was covered with adsorbed oxygen/nitrogen, oxides, hydroxides, and/or organic species after washing them with water or ethanol to remove excess $NaNH_2$ and NaOH byproducts. The excess $NaNH_2$ is the key factor in this meta-synthesis route as this amide works as a molten salt to enhance the kinetics of the reaction and fulfills the thermodynamic requirements in a closed system by forming NaOH as the byproduct. We believe that this low-temperature nitridation technique has the potential to reduce synthesis temperature and usage amount of ammonia for producing functional nitride materials, and that it would facilitate the synthesis of new structures, compositions, and morphologies that are not accessible by the usual high-temperature routes.

dx.doi.org/10.1021/ic401951u | Inorg. Chem. 2013, 52, 11787−11791

AUTHOR INFORMATION

Corresponding Author

*E-mail: amiura@yamanashi.ac.jp. Phone: +81-55-220-8614.

Notes

The authors declare no competing financial interest.

ACKNOWLEDGMENTS

A.M. acknowledges Ms. Chiaya Yamamoto for helping with TEM observations, Mr. Satoki Shinozuka for XPS measurement, and Profs. Nagao Masanori and Satoshi Watauchi for help with magnetic measurements. This work was partially supported by JSPS Grant-in-Aid for Young Scientists (No. 13275194).

REFERENCES

(1) (a) Cameron, J. M.; Hughes, R. W.; Zhao, Y.; Gregory, D. H. *Chem. Soc. Rev.* **2011**, *40*, 4099−4118. (b) DiSalvo, F. J.; Clarke, S. J. *Curr. Opin. Solid State Mater. Sci.* **1996**, *1* (2), 241−249.

(2) Schnepp, Z.; Thomas, M.; Glatzel, S.; Schlichte, K.; Palkovits, R.; Giordano, C. *J. Mater. Chem.* **2011**, *21* (44), 17760−17764.

(3) Dhanasekaran, P.; Salunke, H. G.; Gupta, N. M. *J. Phys. Chem. C* **2012**, *116* (22), 12156−12164.

(4) Houben, A.; Sepelak, V.; Becker, K.-D.; Dronskowski, R. *Chem. Mater.* **2009**, *21* (5), 784−788.

(5) Guo, K.; Rau, D.; Toffoletti, L.; Müller, C.; Burkhardt, U.; Schnelle, W.; Niewa, R.; Schwarz, U. *Chem. Mater.* **2012**, *24* (23), 4600−4606.

(6) (a) Chi, E. O.; Kim, W. S.; Hur, N. H. *Solid State Commun.* **2001**, *120* (7−8), 307−310. (b) Takenaka, K.; Takagi, H. *Appl. Phys. Lett.* **2005**, *87* (26), 261902−3. (c) Takenaka, K.; Hamada, T.; Kasuga, D.; Sugimoto, N. *J. Appl. Phys.* **2012**, *112* (8), 083517.

(7) (a) Ma, S. S. K.; Hisatomi, T.; Maeda, K.; Moriya, Y.; Domen, K. *J. Am. Chem. Soc.* **2012**, *134* (49), 19993−19996. (b) Yang, M.; DiSalvo, F. J. *Chem. Mater.* **2012**, *24* (22), 4406−4409. (c) Wang, H.; Wu, Z.; Kong, J.; Wang, Z.; Zhang, M. *J. Solid State Chem.* **2012**, *194*, 238−244. (d) Schliehe, C.; Yuan, J.; Glatzel, S.; Siemensmeyer, K.; Kiefer, K.; Giordano, C. *Chem. Mater.* **2012**, *24* (14), 2716−2721. (e) Watanabe, T.; Nonaka, K.; Li, J.; Kishida, K.; Yoshimura, M. *J. Ceram. Soc. Jpn.* **2012**, *120* (1407), 500−502. (f) Miura, A.; Shimada, S.; Sekiguchi, T.; Yokoyama, M.; Mizobuchi, B. *J. Cryst. Growth* **2008**, *310* (3), 530−535.

(8) (a) Choi, J.; Gillan, E. G. *Inorg. Chem.* **2009**, *48* (10), 4470−4477. (b) Gu, Y.; Guo, F.; Qian, Y.; Zheng, H.; Yang, Z. *Mater. Lett.* **2003**, *57* (11), 1679−1682. (c) Qian, X. F.; Zhang, X. M.; Wang, C.; Tang, K. B.; Xie, Y.; Qian, Y. T. *Mater. Res. Bull.* **1999**, *34* (3), 433−436. (d) Xie, Y.; Qian, Y.; Wang, W.; Zhang, S.; Zhang, Y. *Science* **1996**, *272* (5270), 1926−1927. (e) Song, B.; Chen, X.; Han, J.; Jian, J.; Wang, W.; Zuo, H.; Zhang, X.; Meng, S. *Inorg. Chem.* **2009**, *48* (22), 10519−10527. (f) Zhang, T.; Kouyama, A.; Sugiura, T. *J. Ceram. Soc. Jpn.* **2012**, *120* (1397), 25−29. (g) Hsieh, J. C.; Yun, D. S.; Hu, E.; Belcher, A. M. *J. Mater. Chem.* **2010**, *20* (8), 1435−1437.

(9) (a) Yang, L.; Yu, H.; Xu, L.; Ma, Q.; Qian, Y. *Dalton Trans.* **2010**, *39* (11), 2855−2860. (b) Jacobs, H.; von Pinkowski, E. *J. Less-Common Met.* **1989**, *146*, 147−160. (c) Rauch, P. E.; DiSalvo, F. J. *J. Solid State Chem.* **1992**, *100* (1), 160−165. (d) Rauch, P. E.; DiSalvo, F. J.; Brese, N. E.; Partin, D. E.; O'Keeffe, M. *J. Solid State Chem.* **1994**, *110* (1), 162−166.

(10) Huang, Y.; Gu, Y.; Zheng, M.; Xu, Z.; Zeng, W.; Liu, Y. *Mater. Lett.* **2007**, *61* (4−5), 1056−1059.

(11) Miura, A.; Takei, T.; Kumada, N. *Cryst. Growth Des.* **2012**, *12* (9), 4545−4547.

(12) Momma, K.; Izumi, F. *J. Appl. Crystallogr.* **2008**, *41* (3), 653−658.

(13) Suzuki, K.; Kaneko, T.; Yoshida, H.; Obi, Y.; Fujimori, H.; Morita, H. *J. Alloys Compd.* **2000**, *306* (1−2), 66−71.

(14) Wang, Z.; Huang, B.; Yu, L.; Dai, Y.; Wang, P.; Qin, X.; Zhang, X.; Wei, J.; Zhan, J.; Jing, X.; Liu, H.; Whangbo, M.-H. *J. Am. Chem. Soc.* **2008**, *130* (48), 16366−16373.

(15) Rosenberger, L.; Baird, R.; McCullen, E.; Auner, G.; Shreve, G. *Surf. Interface Anal.* **2008**, *40* (9), 1254−1261.

(16) Bertóti, I. *Surf. Coat. Technol.* **2002**, *151*−*152*, 194−203.

(17) Podgornov, E. A.; Prosvirin, I. P.; Bukhtiyarov, V. I. *J. Mol. Catal. A: Chem.* **2000**, *158* (1), 337−343.

(18) (a) Stranick, M. A. *Surf. Sci. Spectra* **1999**, *6* (1), 39−46. (b) Tang, X.; Li, J.; Sun, L.; Hao, J. *Appl. Catal., B* **2010**, *99* (1−2), 156−162.

(19) Torres, J.; Perry, C. C.; Bransfield, S. J.; Fairbrother, D. H. *J. Phys. Chem. B* **2003**, *107* (23), 5558−5567.

(20) Zhang, Z.; Lu, J.; Yun, T.; Zheng, M.; Pan, J.; Sow, C. H.; Tok, E. S. *J. Phys. Chem. C* **2013**, *117* (3), 1509−1517.

(21) (a) Wang, Y.; Lesterb, E.; Gregory, D. *J. Mater. Sci.* **2007**, *42* (16), 6779−6786. (b) Ohashi, Y.; Motohashi, T.; Masubuchi, Y.; Moriga, T.; Murai, K.; Kikkawa, S. *J. Solid State Chem.* **2011**, *184* (8), 2061−2065.

(22) Leineweber, A.; Niewa, R.; Jacobs, H.; Kockelmann, W. *J. Mater. Chem.* **2000**, *10* (12), 2827−2834.

(23) Liapina, T.; Leineweber, A.; Mittemeijer, E. J.; Kockelmann, W. *Acta Mater.* **2004**, *52* (1), 173−180.

(24) Zhong Qing, Y.; Jian Rong, Z.; You Wei, D. *J. Magn. Magn. Mater.* **1996**, *159* (1−2), L8−L10.

(25) Kurian, S.; Gajbhiye, N. S. *J. Nanopart. Res.* **2009**, *12* (4), 1197−1209.

(26) Lu, D.; Hitoki, G.; Katou, E.; Kondo, J. N.; Hara, M.; Domen, K. *Chem. Mater.* **2004**, *16* (9), 1603−1605.

(27) Wang, S.; Zhang, Z.; Zhang, Y.; Qian, Y. *J. Solid State Chem.* **2004**, *177* (8), 2756−2762.

(28) Elder, S. H.; DiSalvo, F. J.; Topor, L.; Navrotsky, A. *Chem. Mater.* **1993**, *5* (10), 1545−1553.

(29) *CRC Handbook of Chemistry and Physics*, 83*rd ed.*; CRC Press: Boca Raton, FL, 2002; Vol. 83, pp 5-5−5-50.

(30) Tessier, F.; Navrotsky, A.; Niewa, R.; Leineweber, A.; Jacobs, H.; Kikkawa, S.; Takahashi, M.; Kanamaru, F.; DiSalvo, F. J. *Solid State Sci.* **2000**, *2* (4), 457−462.

(31) (a) Miura, A.; Shimada, S. *Mater. Res. Bull.* **2006**, *41* (9), 1775−1782. (b) Miura, A.; Shimada, S.; Sekiguchi, T. *J. Cryst. Growth* **2007**, *299* (1), 22−27.